THE ASTROPHYSICAL JOURNAL, 444:748–757, 1995 May 10

HOPKINS ULTRAVIOLET TELESCOPE OBSERVATIONS OF H_2 TOWARD THE PLANETARY NEBULA NGC 1535

CHARLES W. BOWERS,[1] WILLIAM P. BLAIR,[2] KNOX S. LONG,[3] AND ARTHUR F. DAVIDSEN[2]
Received 1993 November 15; accepted 1994 November 11

ABSTRACT

We have observed the far-ultraviolet spectrum (912–1860 Å) of the bright high-excitation planetary nebula NGC 1535 with ~3 Å resolution using the Hopkins Ultraviolet Telescope aboard the Astro-1 space shuttle mission in 1990 December. We see strong continuum emission down to the Lyman limit and strong P Cygni profiles from high-excitation lines such as C IV λ1549, N V λ1240, O V λ1371, and O VI λ1035. Below 1150 Å strong absorption bands of H_2 are seen, which were unanticipated by us because of the low reddening and high galactic latitude of the object and the absence of detected H_2 emission in the infrared. We construct model H_2 spectra and convolve them to the HUT resolution for comparison with the NGC 1535 data. We find good agreement with a population distribution characterized by a single temperature ($T = 300$ K) or a two-temperature model ($T = 144/500$ K), and determine limits on the H_2 column density. While both interstellar and circumstellar origins for the observed H_2 absorption are plausible, we ascribe the material to the planetary nebula in order to estimate the conditions of excitation and place upper limits on the mass of both H_2 and H I in this system. Because the UV transitions are ground-state connected, we determine a stringent upper limit of $0.03 d_{1.6}^2\ M_\odot$ on the mass of H_2, where $d_{1.6}$ is the distance relative to an assumed distance of 1.6 kpc. This value is less model-dependent than IR estimates. Along with the central star and nebular masses, these estimates allow us to limit the main-sequence mass of the progenitor star to less than 1.8 $M_\odot$. This upper limit is consistent with a relatively low-mass extended thick disk or Population II progenitor, as expected for an object ~1 kpc off the galactic plane.

Subject headings: ISM: molecules — planetary nebulae: individual (NGC 1535) — ultraviolet: ISM

1. INTRODUCTION

Planetary nebula central stars provide an important link in the chain of stellar evolution and play an important role in the dynamics and evolution of the surrounding planetary nebula (PN) through photoionization and by producing a strong stellar wind. Following nebular ejection, the hot core cools (rapidly at first) along tracks in the H-R diagram such as those calculated by Schönberner (1981, 1983). The spectral region between Lyα and the Lyman limit at 912 Å has been observed for only a few PNs at low resolution with the *Voyager* Ultraviolet Spectrometer (Polidan & Holberg 1985). This spectral region is of great interest; the spectra of these hot central stars rise rapidly into the far-UV, so more leverage for temperature determinations is possible in spectra that extend to the Lyman limit. For central stars with winds, this spectral band includes the important doublet of O VI λλ1032, 1038, which accesses a hotter portion of the wind than other UV lines. Also, the region below 1150 Å contains the Lyman and Werner bands of molecular hydrogen. These transitions are ground-state connected, making them sensitive to very low column densities of H_2.

H_2 has been observed by way of IR emission in a number of PNs (Treffers et al. 1976; Beckwith, Persson, & Gatley 1978; Isaacman 1984; Storey 1984; Zuckerman & Gatley 1988). It is the dominant form of hydrogen in the stellar wind in the early, superwind phase of asymptotic giant branch (AGB) mass loss (Howe, Millar, & Williams 1992). A substantial amount of mass in PNs can remain in the form of H_2 into the PN phase. For example, Sahai et al. (1991) have estimated that as much as 3 $M_\odot$ of H_2 is present in IC 4406. H_2 can be dissociated to H I by shocks or by photodissociation by radiation from the PN central star longward of 912 Å through Lyman and Werner band absorption. Thus a neutral zone of mixed H I and H_2 can be formed around the ionized nebula, making it ionization bounded. This neutral region can have as much or greater mass than the ionized gas. The existence of substantial quantities of neutral gas in some objects could help explain the apparent discrepancy between the sum of the central star mass (typically 0.58 $M_\odot$; see Schönberner 1981) and ionized mass (typically a few tenths to 1 $M_\odot$; see Pottasch 1984) and the much larger range of progenitor masses, believed to extend to at least 5 $M_\odot$ (Heap & Augensen 1987). Measurement of the neutral gas mass in PNs, combined with determinations of central star and ionized mass, permits the total progenitor mass to be established. This provides a direct check on theories of post-AGB evolution.

The methods used previously to determine the mass of H_2 in PNs involve uncertain extrapolations. Infrared H_2 emission only measures the small amount of gas in excited states; the total H_2 present must be estimated from models of the excitation mechanism, either shock heating (Isaacman 1984) or fluorescence (Dinerstein et al. 1988). An alternative approach has been to measure CO emission in PNs. To estimate the bulk of molecular gas in the form of H_2, a CO/H_2 ratio must be assumed. Such an estimate is invalid in any region where H_2 and CO are not coexistent (for instance, where self-shielding causes differences in their spatial extent), so these estimates provide lower limits only (Huggins & Healy 1989; Sahai et al.

[1] Laboratory for Astronomy and Solar Physics, Code 683.3, NASA Goddard Space Flight Center, Greenbelt, MD 20771.
[2] Department of Physics and Astronomy, Johns Hopkins University, Charles & 34th Streets, Baltimore, MD 21218.
[3] Space Telescope Science Institute, 3700 San Martin Drive, Baltimore, MD 21218.

1991). By having spectroscopic access to the 900–1100 Å region, absorption from the Lyman and Werner bands provides a means of directly sampling the major component of molecular gas in PNs in its most abundant state.

NGC 1535 is a moderately high-excitation PN (class 7; Pottasch 1984) with a bright inner region $\sim 20''$ in diameter surrounded by a much fainter and lower excitation halo with diameter $\sim 60''$ (see Fig. 1). The inner bright region expands at about 20 km s^{-1} and the outer halo expands at roughly half this value (Sabbadin, Bianchini, & Hamzaoglu 1984). The extinction to NGC 1535 is low, with $E(B-V) \leq 0.1$ (Pottasch 1984, and references therein). At $\alpha(1950) = 04^h11^m57^s$ and $\delta(1950) = -12°51'42''$, the line of sight to NGC 1535 passes well out of the Galactic plane ($l^{II} = 206°$, $b^{II} = -40°$). Distance estimates for NGC 1535 are summarized by Sabbadin et al. (1984) and range from 0.79–3.13 kpc. We adopt $d = 1.6$ kpc, which corresponds to a z distance of ~ 1 kpc. The central star of this PN is bright, with $V \cong 12.0$ (Adam & Köppen 1985, and references therein), a temperature near 70,000 K (determined both from analysis of the hydrogen Balmer line profiles and nebular emission line fluxes—see Aller 1982; Méndez et al. 1988; Patriarchi, Perinotto, & Cerruti-Sola 1989), and a mass near 0.67 $M_\odot$ (Méndez et al. 1988). At the assumed distance, the luminosity of the central star is $\sim 10^4\ L_\odot$. The low extinction and high temperature makes this central star an excellent source for observation in the far-UV.

Below we describe an observation of NGC 1535 made with the Hopkins Ultraviolet Telescope (HUT) during the Astro-1 space shuttle mission (STS-35) in 1990 December. We focus on the largely unexplored region between 1150 Å and the Lyman limit at 912 Å. A very strong P Cygni profile due to O VI $\lambda\lambda$1032, 1038 is seen in this spectral region. Also, atomic hydrogen and the H_2 Lyman and Werner bands absorb strongly in this spectral region and their distinctive absorption pattern is clearly detected against the continuum flux of the central star. We present measurements of this absorption spectrum and compare it to a series of model H_2 spectra convolved to the HUT resolution. This comparison enables us to derive limits on the population distribution among rotational states and the column density of H_2. With this information, we estimate the total H_2 mass along this line of sight. We also estimate the H I mass and infer an upper limit to the mass of the stellar progenitor of this PN. In § 2 we describe the observations and data reduction procedures, while in § 3 the H_2 models and model fitting are discussed. Finally, in § 4 we derive an upper limit on the mass of H_2 and discuss the implications of these results for the precursor star of NGC 1535.

2. OBSERVATIONS AND DATA REDUCTION

HUT consists of an f/2–0.9 m mirror that feeds a prime focus spectrograph with a microchannel-plate intensifier and photon-counting detector. In first order the spectrograph covers the region from 830 to 1860 Å at 0.51 Å $pixel^{-1}$ with a nominal resolution of ~ 3 Å. The aperture plate can be rotated to permit various apertures to be selected for use in observations. Details of the calibration and the telescope performance on orbit can be found in Davidsen et al. (1992) and Kimble et al. (1993).

The HUT observation of NGC 1535 used a $9\farcs4 \times 116''$ slit at a position angle of 335°, and was obtained on 1990 December 7 beginning at 23:49 GMT for a total of 1752 s. The HUT aperture is shown in projection on Figure 1 (Plate 16), which is a [N II]λ6584 image of the nebula provided by B. Balick (see Balick 1987 for details). Note that Balick et al. (1992) have searched for evidence of a more extended outer halo in NGC 1535 without success. The entire HUT observation occurred during orbital night, when residual airglow emissions are weakest. The aperture was positioned relative to preplanned guide stars using the HUT acquisition TV camera, which views the slit plane; the aperture position could be verified visually since the central star and inner nebula were clearly visible on the acquisition TV. The slit was placed on the central star for the first 700 s of the observation and then repositioned to obtain a nebular spectrum. Here we report only the spectrum of the central star. Pointing stability during this portion of the observation was $\sim 4''$ rms, although several excursions of order $10''$ were noted.

The data were converted to IRAF[4] file format for reduction and processing. The raw data have about 750 counts per 0.51 Å bin near 1000 Å. Corrections were applied to remove dark count and pulse persistence from the phosphor readout of the detector. Because the object was quite bright and airglow contamination relatively weak, no airglow correction, either in emission lines or as grating scattered light, has been applied. The wavelength stability of the HUT spectrograph is excellent, and conversion from pixel space to wavelengths was straightforward. The HUT flux calibration is based on a comparison between the observed spectrum of the DA white dwarf G191−B2B and a model atmosphere, as well as preflight and postflight laboratory calibration (see Davidsen et al. 1992). Local variations in the calibration of order $\pm 5\%$ may still exist.

Figure 2 shows the resulting flux-calibrated spectrum in comparison to a 70,000 K non-LTE model from Clegg & Middlemass (1987). The model points are shown as diamonds and the smooth curve is a spline function fit to these points. The data have been corrected for extinction using the standard Galactic extinction curve of Seaton (1979) as extended to short wavelengths by Longo et al. (1989). Normalizing at 1450 Å, a value of $E(B-V) \sim 0.1$ is required to match the data to this model. The spectrum consists of the central star continuum, strong P Cygni profiles of C IV λ1549, N V λ1240, O V λ1371, and O VI $\lambda\lambda$1032, 1038, nebular emission at He II λ1640, and interstellar absorption lines such as O I/Si II λ1302, Si II λ1262, and C II λ1335.

In addition to the P Cygni lines, tremendous structure is seen in the spectrum below 1150 Å; a series of absorption features is present with depths ranging from about 10% to nearly 50% of the continuum. In Figure 3 we display the spectrum below 1150 Å enlarged to show this structure. (These data are shown before reddening correction.) We indicate on Figure 3 the positions of the Lyman series of atomic hydrogen and the Lyman ($X^1\Sigma_g^+ - B^1\Sigma_u$) and Werner ($X^1\Sigma_g^+ - C^1\Pi_u$) bands of molecular hydrogen. The molecular line positions shown in Figure 3 are those of the strong $R(0)$ ($J'' = 0$, $J' = 1$) rotational transitions between the ground vibrational state ($v'' = 0$) and the upper vibrational states indicated. The coincidence between the absorption features and the molecular transitions indicated clearly shows that H_2 is present along the line of sight to NGC 1535. Also, the atomic hydrogen lines are clearly present in the stellar spectrum. A broad stellar Lyα absorption

[4] IRAF is distributed by the National Optical Astronomy Observatories, which is operated by the Association of Universities for Research in Astronomy, Inc. (AURA) under cooperative agreement with the National Science Foundation.

PLATE 16

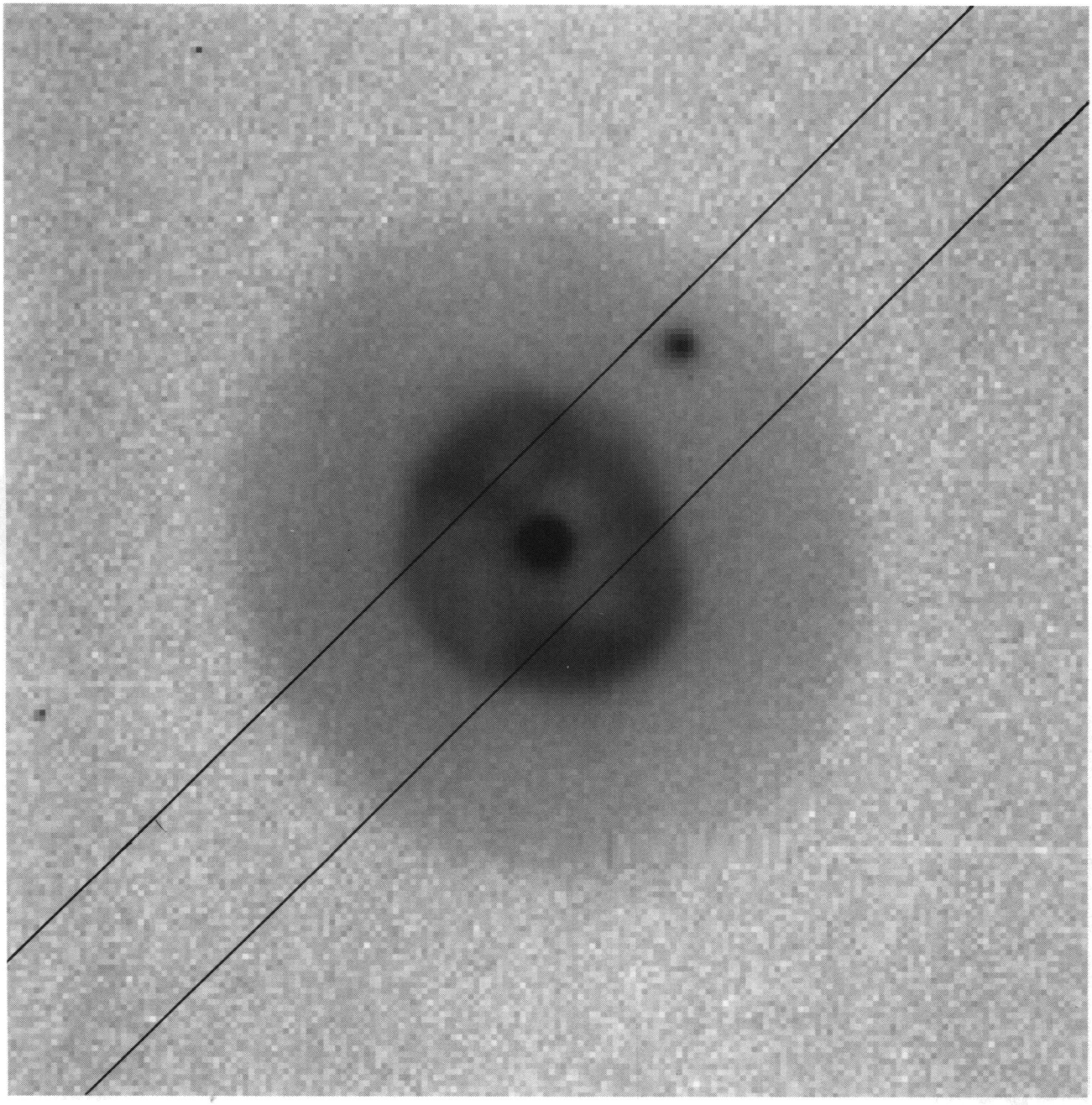

FIG. 1.—CCD image of NGC 1535 in the light of [N II]λ6584, obtained at the KPNO 2.1 m telescope with a 15 Å FWHM filter centered at 6585 Å (Balick 1987). The HUT 9.″4 × 116″ aperture is shown in projection although the long dimension overfills the figure. The region shown is approximately 72″ on a side. North is up, east to the left. (Data provided by Bruce Balick.)

BOWERS et al. (see 444, 749)

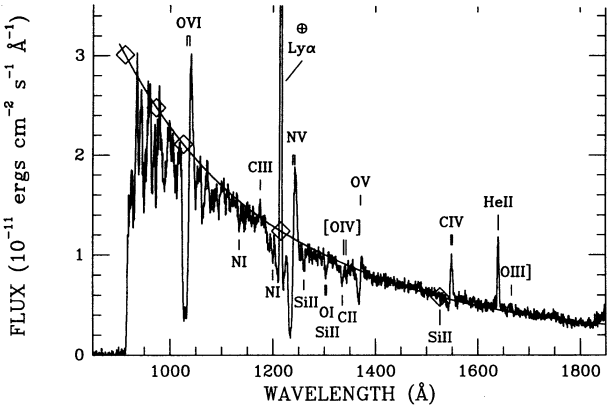

FIG. 2.—Flux-calibrated HUT spectrum of the central star of NGC 1535. This Figure shows the entire range observed by HUT after correction for $E(B-V) = 0.1$ (see text). Note the rising continuum to shorter wavelengths and the strong P Cygni profiles due to C IV, N V, O V, and O VI, indicating a strong wind from the central star. The diamonds show a 70,000 K model from Clegg & Middlemass (1987) scaled to the data at 1450 Å. A smooth spline curve is fit through these points to provide a reference.

is seen, although contamination from the geocoronal emission and the N V P Cygni line is present. Lyβ is blended with the P Cygni absorption component of O VI, and absorptions are seen at the positions of Lyγ, Lyδ, and Lyϵ as well (although blending with molecular transitions is also occurring).

3. ANALYSIS AND MODEL FITTING

The Lyman and Werner band absorption spectrum of H_2 has average line separations of a few hundred mÅ, much less than the HUT resolution of ~3 Å. Thus the HUT spectrum of H_2 absorption toward NGC 1535 consists of a series of features, as illustrated in Figure 3, each of which is composed of many unresolved lines. For this reason, we cannot resolve interstellar or nebular H_2 components, nor can we measure the individual line equivalent widths to determine the population distribution among levels of the excitation conditions. Instead we synthesize model spectra and compare these models to our observed spectrum. This permits us to limit the possible distribution of population among the H_2 rotational levels and determine an acceptable range for the H_2 column density.

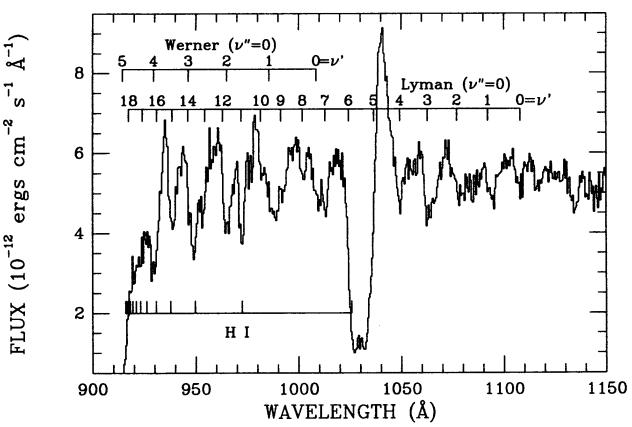

FIG. 3.—Enlarged portion of the observed spectrum (i.e., before reddening correction) below 1150 Å. The hydrogen Lyman series lines are indicated, as are the Lyman and Werner bands of molecular hydrogen. Both atomic and molecular hydrogen lines are prominent in absorption against the central star.

3.1. H_2 *Model Calculations*

In order to model the effects of H_2 absorption we have followed the procedure outlined by Cartwright & Drapatz (1970) and used the wavelengths and oscillator strengths from Morton & Dinerstein (1976). Our models include 420 lines comprising the Lyman ($v'' = 0$, $v' = 0$–20, $J'' = 0$–7) and Werner ($v'' = 0$, $v' = 0$–6, $J'' = 0$–5) series of transitions from the electronic and vibrational ground state. The input parameters of each model are the column densities of the above rotational levels and the gas turbulent velocity, expressed as the Doppler velocity parameter, b. We also investigated deviations of the H_2 ortho–para ratio from the thermal equilibrium 3:1 ratio but found no measurable effects at our resolution. Optical depths were calculated using Voigt profiles at 1 mÅ intervals. The corresponding transmission function was then computed, smoothed, and binned to 0.51 Å to match the HUT resolution and pixel size.

Although models were constructed over the full wavelength range of observable molecular hydrogen absorption, roughly 912–1108 Å, for several reasons detailed comparison to the data have been made over just the 980–1020 Å region. This region is broad enough so that five distinct H_2 features are present ($\lambda\lambda$986, 992, 1002, 1010, and 1013), formed from transitions of both the Lyman and Werner series. Our H_2 absorption models show a signficant variation with rotational level temperature in the relative depths of these five H_2 absorption features. Restricting our attention to this 40 Å band also minimizes the effects of possible variations in the stellar continuum, the assumed $E(B-V)$ to NGC 1535, the poorly known FUV extinction law, and any instrumental calibration uncertainties that may remain. Within this 40 Å band, only the region from about 987–982 Å is corrupted by effects other than pure H_2 absorption. These effects include strong IS absorption from the O I resonance triplet near 988.7 Å, terrestrial airglow emission from the same O I transitions, and N III λ991 (the only strong nebular emission expected in the 980–1020 Å region). Rather than attempting to model all of these effects, we ignore this 5 Å region near 989 Å.

To validate our modeling procedure, we constructed a model of the H_2 absorption spectrum toward the O9.5 Ia star α Cam (HD 30614), which was observed both with HUT during Astro-1 and at much higher resolution with the *Copernicus* satellite (Spitzer, Cochran, & Hirshfeld 1974; Savage et al. 1977). The HUT observation of α Cam occurred on 1990 December 8 at 17:57 UT; we use a portion of this data about 1600 s in length, also obtained during orbital night, although an 18″ circular aperture was in place instead of the long slit used for the NGC 1535 observation. The pointing was somewhat erratic, producing a nonphotometric spectrum. The resulting spectral resolution was about 3.5 Å. These data were reduced in a manner similar to that described above for NGC 1535. Figure 4 shows an appropriate portion of the flux calibrated α Cam spectrum after correcting for a color excess of $E(B-V) = 0.32$ (Savage et al. 1977) using the extinction curve derived from Longo et al. (1989).

The results of the *Copernicus* analyses of the H_2 level populations in α Cam were used to construct an absorption model using the program described above. The total H_2 column density modeled was 2.2×10^{20} cm^{-2} with a Doppler b parameter of 8.5 km s^{-1} (Spitzer et al. 1974; Savage et al. 1977). The rotational level population distribution was obtained from the *Copernicus* analyses. The resulting model

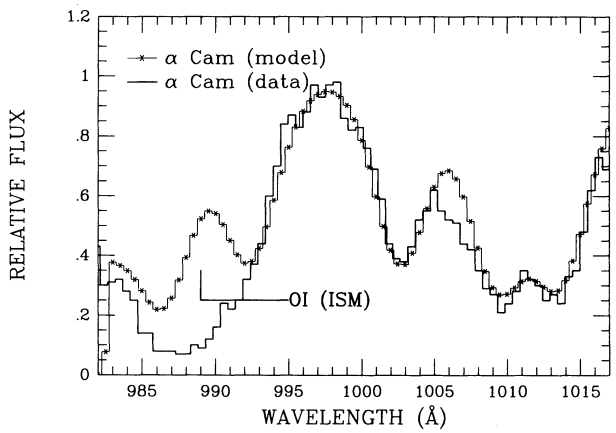

FIG. 4.—Comparison of HUT spectrum of the O9.5 Ia star α Cam with an H_2 absorption model calculated with the level populations derived from *Copernicus* data (Spitzer et al. 1974; Savage et al. 1977). The stellar spectrum has been corrected for $E(B-V) = 0.32$ (see text). The region of discrepancy near 989 Å is due to geocoronal and nebular emission and IS absorption from O I λ989 not incorporated into the model.

H_2 absorption spectrum was smoothed using a Gaussian function with FWHM = 3.5 Å in order to match the HUT resolution for this observation. The resulting model is shown against the data in Figure 4. No correction for a sloping spectral continuum over this limited wavelength range has been applied. The model spectrum matches the data very closely with the exception of two discrepant areas: the O I λ989 IS absorption feature is clearly evident in the data, and there is a small flux excess in the model near 1006 Å. A small (<30%) amount of this latter difference may be due to IS absorption by Cl I λ1004.7 (Morton 1991) using the column toward α Cam of 1.1×10^{14} cm^{-2} (Harris & Bromage 1984). The remaining cause of the discrepancy near 1006 Å is still unknown, with the likely sources being an unknown absorption feature or an error in the relevant H_2 oscillator strengths. The agreement elsewhere is very good. We conclude that our modeling procedure is adequate and proceed with models of NGC 1535.

3.2. *Modeling Parameters*

Each of the H_2 absorption features observed at our resolution is composed of several individual lines of varying strengths. Models with low column density ($\leq 10^{14}$–10^{15} cm^{-2}) in which the H_2 absorption lines lie on the linear portion of the curve of growth (and thus are independent of b), cannot produce sufficient absorption to match the features in our spectrum. To match these, the stronger lines must be on the flat or square root portion of the curve of growth. For a given b, we can adjust the total H_2 column density, sliding the lines of a feature along the curve of growth, until the total equivalent width is matched. The range of allowable b-values thus translates into a range of column density. We have also assumed that a single value of b is sufficient to characterize conditions along this line of sight. We now consider appropriate ranges of b assuming alternatively that the observed H_2 is of interstellar or nebular origin.

One estimate of the range of b-values is obtained by considering the H_2 to be of interstellar origin. Luhman & Dinerstein (1990) measured a number of interstellar species along the line of sight to NGC 1535 and obtained a consistent curve of growth with $b = 15.8$ km s^{-1} using a number of ions. The value of b for most of the H_2 column along the line of sight to the nearby star HD 28497 was also estimated to lie between 7 and 15 km s^{-1}. We thus assume that b may extend from 7–15.8 km s^{-1} provided the H_2 is of interstellar origin.

While direct measurements of b in a PN H_2 region have not been reported, we can estimate a probable range of b from H I and CO measurements which should be co-spatial with H_2. The few IR images of H_2 emission over a PN have shown that this neutral zone is typically a shell located at the periphery of the ionization region (Zuckerman & Gatley 1988). In most CO emission (Huggins 1989) and H I absorption (Taylor, Gussie, & Pottasch 1990) measurements that have been made, the PNe underfill the beam size. The resulting line profiles are thus composed of both the neutral shell expansion velocity and the characteristic turbulent velocity. Both CO and H I studies present profiles with widths typically similar to the ionized nebular velocity. Both studies thus conclude that the neutral region expansion velocity is comparable to the ionized zone expansion velocity; under this condition, the turbulent velocity must be considerably less than the expansion velocity in order to produce negligible broadening of the profile. In the case of NGC 6072 (Huggins & Healy 1989), whose extent is over twice the beamwidth, the CO emission profile consists of advancing and receding portions of the neutral shell at about 17 km s^{-1} with a velocity distribution (FWHM) of about 7 km s^{-1}. Sabbadin et al. (1984) have determined that the nebular halo of NGC 1535 has an expansion velocity of about 10 km s^{-1}. We will assume that any associated H_2 is likely to be found near the edge of the nebular halo with a comparable expansion velocity of 10 km s^{-1}. We then conservatively estimate a range of turbulent velocity (FWHM) from 4–10 km s^{-1} leading to a likely b range of 3–7 km s^{-1}. We note that the corresponding b of H_2 at a temperature of 1500 K, typically estimated for shock heating of nebular H_2, is 3.5 km s^{-1}.

To synthesize a model H_2 spectrum, we must also specify the population distribution among the various J'' rotational levels of the $v'' = 0$, ground vibrational state. In order to keep the number of combinations manageable and to use physically meaningful distributions, we have used some simple characterizations which are in broad agreement with both observations and models. These consist of distributing the population according to a single rotational temperature or by two different temperature distributions, one over the rotational levels $J'' = 0$–2 and the second over levels 3–7.

Studies of the H_2 absorption spectra from *Copernicus* have shown that interstellar H_2 has two distinctive population distributions, each producing characteristic spectra (Spitzer & Cochran 1973). In those cases where $N(0)$ (the population in the $J'' = 0$ level) exceeded 10^{17} cm^{-2}, the $N(J)$ population drops sharply to level $J'' = 2$ or 3, and is well characterized by a mean temperature of 77 ± 17 K (Savage et al. 1977). The population of the higher levels drops less rapidly, with a temperature of 180–390 K. For those cases where $N(0) < 10^{15}$ cm^{-2}, a single high temperature of 300–1100 K suffices to describe the entire population distribution to level 3 or 4.

The population distribution among H_2 levels near PNs is less certain and depends on the excitation mechanism. Various authors have interpreted the results of IR measurements of nebular H_2 in terms of shock excitation of the molecular gas (Beckwith et al. 1980; Isaacman 1984). Such gas would have a thermalized population distribution with characteristic temperatures inferred from the IR measurements of 1000–2000 K. However, fluorescent excitation of H_2 may also occur near a strong photoionizing source like the hot central star of a PN

(Dinerstein et al. 1988). Fluorescent emission probably occurs in photodissociation regions (PDRs), relatively dense regions (10^3–10^7 cm^{-3}) near a strong photoionizing source (Sternberg & Dalgarno 1989; Burton, Hollenbach, & Tielens 1990). In PDRs at low densities, the lowest J'' rotational levels of the ground vibrational state are thermalized (up to a few hundred K) by collisions with hot photoelectrons ejected from dust in the PDR. The higher J'' levels follow a distribution that may be characterized by a much higher temperature, up to several thousand K, though such a break is most evident at higher J'' values where our observations are not applicable. This distribution is established by the UV pumping rate and relatively high transition probabilities for these levels. At high densities in a PDR, a thermalized distribution is established with a single high temperature, typically several hundred K.

3.3. H_2 *Modeling Results*

A series of model H_2 absorption spectra were produced with the procedures and parameters just described. Each spectrum generated was smoothed with a Gaussian of full width at half-maximum 2.5 Å, a value which was determined to best match the data in the 980–1020 Å region. For a specific b-value and population distribution, the total column density was varied to provide the best overall fit to the data. The ability of the models to reproduce our spectrum was determined largely by eye, using not only the apparent match between the model and data but by judging the divided spectrum for smoothness. This latter technique is similar to that used to evaluate *Copernicus* observations of H_2 absorption (Savage et al. 1977).

In a limited number of cases, χ^2 minimization fits were also performed. Since the HUT detector is photon counting, it is straightforward to generate and propagate an error array for each observation. A routine called "specfit," developed by G. Kriss and integrated into IRAF, was used with the data and error arrays and assumed model parameters to produce fits for which χ^2 was minimized (Kriss 1995). For a specified b and population distribution, a series of models with different total column densities was generated. Specfit was then applied, interpolating between models to determine the column density that minimized χ^2. A blackbody continuum spectrum of 70,000 K and extinction following the law of Longo et al. (1989) were also assumed. Specfit determined the optimal flux normalization and value of extinction over the range $E(B-V) = 0.0$–0.1. The region near the O I λ989 feature was excluded from the fits. This procedure provided a check on the accuracy of the qualitative conclusions and permitted a more accurate determination of the optimal column density.

There are five major H_2 absorption features seen in the 980–1020 Å region as illustrated in Figure 5, at approximately 986 Å, 992 Å, 1010 Å, and 1013 Å. The positions of these features correspond closely to strong absorption lines from the lowest $J'' = 0$, 1 levels indicating their dominance of the population distribution, as expected. Another significant (though small) feature in our data lies at 997 Å, and results from absorption by a significant population in levels $J'' = 3$ and 5. Our data show only a slight indentation in the apparent continuum at this position. The shallowness of this feature provides a major constraint on high temperatures that increase the population in $J'' = 3$ and 5.

Figure 5, comparing our observed spectrum to three models at $b = 15.8$ km s^{-1}, also indicates that the relative depths of the major features in the 980–1020 Å region change with the population distribution, here characterized by three

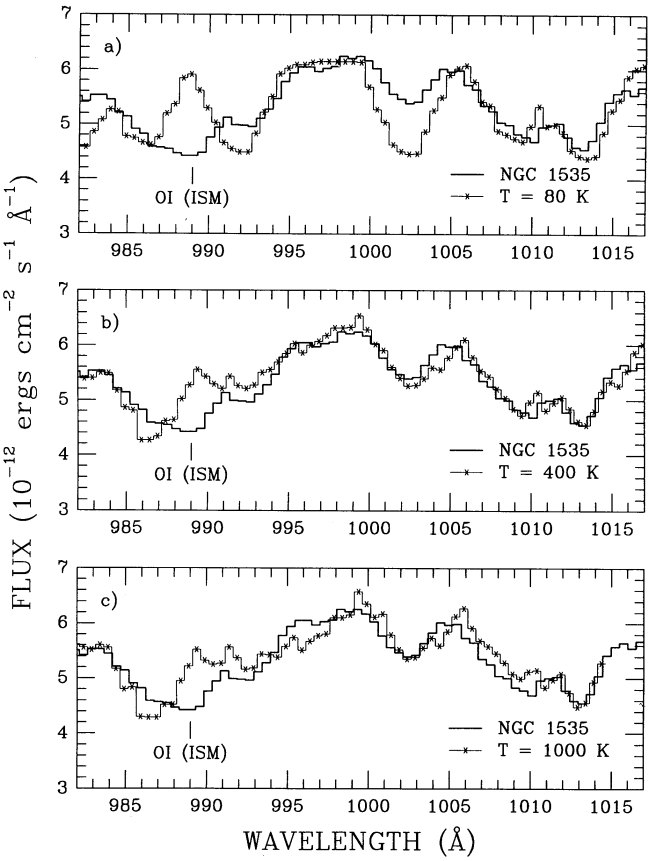

FIG. 5.—Comparison of HUT NGC 1535 spectrum to single-temperature H_2 models. The three models shown are for (*a*) $T = 80$ K, (*b*) 400 K, and (*c*) 1000 K, and the Doppler b parameter is assumed to be 15.8 km s^{-1}. Variations in the b parameter produce relatively minor effects on the best-fit model.

single temperatures, 80, 400, and 1000 K. The 80 K distribution provides a poor match to the data, the modeled 1002 Å feature being much too deep relative to the other major features. At 400 K all of the major features are well matched with $N(H_2) = 2.5 \times 10^{16}$ cm^{-2}, though there is some additional absorption seen at 987 Å that is not present in the data. At 1000 K, the depth of the minor feature at 997 Å, due to the increased population in levels $J'' = 3$ and 5, causes a significant depression not present in our data. We also note in all three models the lack of H_2 absorption at 989 Å, where strong interstellar O I absorption occurs (as seen in our α Cam comparison spectrum, Fig. 4). The difference near 1005 Å seen in α Cam is less apparent in the NGC 1535 models, suggesting the possible presence of additional weak atomic lines visible in the much higher column toward α Cam.

These same general trends are seen throughout the b range that we have investigated, i.e. the best fits are obtained with a single temperature distribution near several hundred degrees. χ^2 minimization was performed on a number of models at $b = 7$ km s^{-1}, with the best fit obtained for the 300 K model and a column density of 7.5×10^{17} cm^{-2}. χ^2 per degree of freedom was 1.57 with 58 degrees of freedom. The data are consistent with a standard deviation of about 5.5% instead of the photon number deviation of about 3.5%. As discussed earlier, a number of factors could account for the fact that χ^2 is this large. For instance, small variations from our assumed extinction law could cause systematic errors and drive up χ^2.

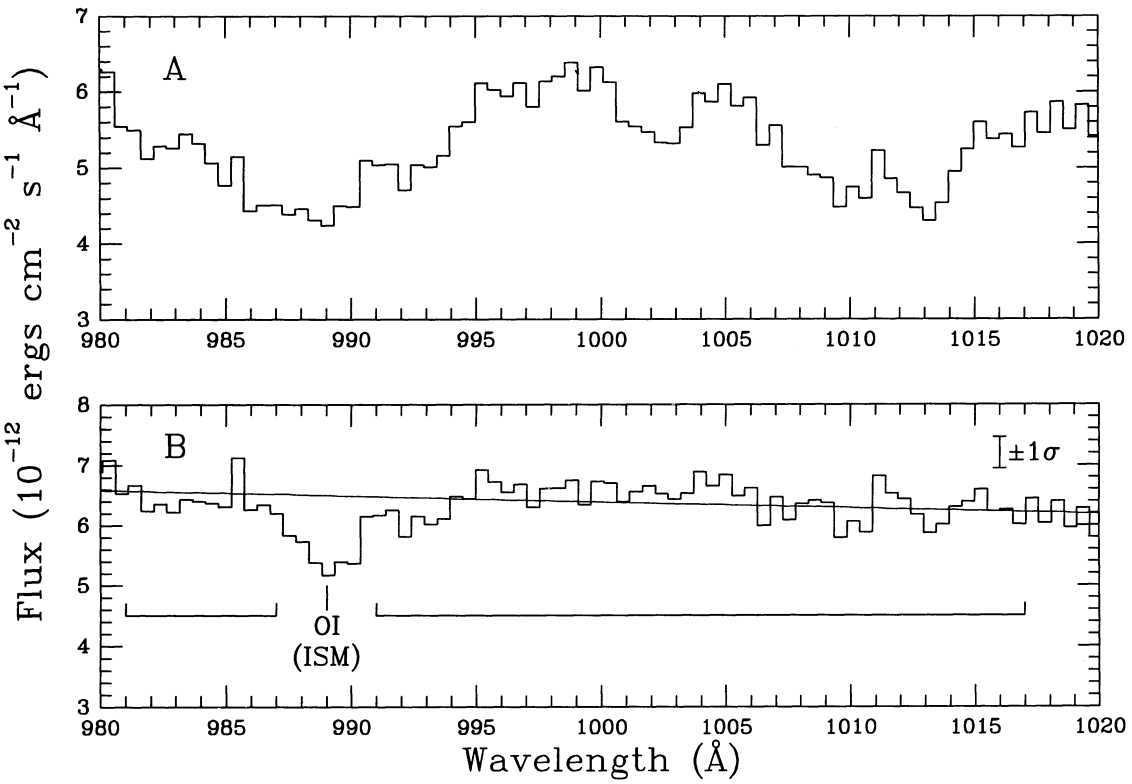

FIG. 6.—Comparison of the original data and the spectrum divided by the best-fit transmission model. Panel (*a*) shows the original spectrum from 980–1020 Å. Panel (*b*) shows the same spectrum after division by the model H_2 transmission for a $b = 7$ km s^{-1} model with $N(H_2) = 7.5 \times 10^{17}$ cm^{-2}. The modeled continuum flux is indicated by the continuous line. The brackets indicate the spectral region included in χ^2 minimization and the error bar at right shows typical ± 1 σ error bars based only on the number of detected photons per 0.51 Å bin.

Figure 6 shows the original data for this optimum model (panel *a*) and the data divided by the modeled H_2 transmission function (panel *b*), which is essentially flat. Also illustrated is the reddened continuum level for this model for comparison. The O I λ989 feature is the largest deviation from a smooth continuum level; the combination of interstellar absorption and airglow emission has resulted in a net absorption in this case.

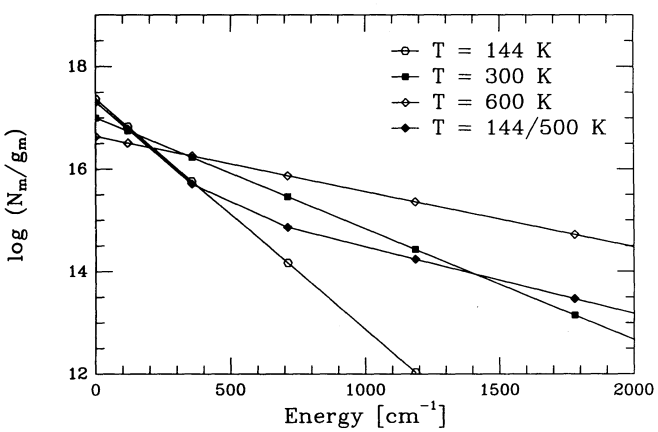

FIG. 7.—Several population distributions which were modeled at $b = 7$ km s^{-1}. The best fits are obtained at $T = 300$ K and the two-temperature $T = 144/500$ K models. These result in the same reduced χ^2 and are indistinguishable, indicating the range of acceptable fits. The two other distributions shown are significantly different and do not produce acceptable fits to the data.

In summary, we find that a population distribution with a single temperature of 300 K provides acceptable fits throughout the b range 3–15.8 km s^{-1}. Over the b range 7 km s^{-1} $\leq b \leq$ 15.8 km s^{-1}, which corresponds to the likely range for an interstellar origin, we find 2.5×10^{16} cm^{-2} $\leq N(H_2) \leq$ 7.5×10^{17} cm^{-2}. Over 3 km s^{-1} $\leq b \leq$ 7 km s^{-1}, corresponding to a nebular origin, we find 7.5×10^{17} cm^{-2} $\leq N(H_2) \leq$ 2.5×10^{18} cm^{-2}. Low temperatures generate models in which the relative depth of the major features are poorly matched. High-temperature models produce too much absorption from $J'' = 3$ and 5 levels, causing a depression near 997 Å. As illustrated in Figure 7, two-temperature distributions that resemble a single temperature distribution of 300 K can also consistently produce reasonable fits to the data.

4. DISCUSSION

Our modeling indicates that population distributions representative of temperatures near several hundred degrees can produce a reasonable fit to our observation. Single-temperature models of 1000–2000 K, which would be expected for shock-heated H_2 near NGC 1535 or which have been frequently observed along low column density lines of sight in the ISM, are clearly excluded. However, some low column density ISM lines of sight have been observed with temperatures as low as about 300 K (Spitzer & Cochran 1973; Spitzer et al. 1974), a condition which would be in a nominal agreement with our data at the lower column densities derived.

We note the broad range of H_2 columns allowed at $E(B-V) = 0.1$ by Savage et al. (1977). However, characteristic

high column density interstellar H_2 models do not agree with our data; the lower $J'' = 0$–2 levels would be expected to have populations characterized by a nominal temperature of 77 K, producing an absorption spectrum similar to the 80 K model shown in Figure 3*a* for the α Cam distribution ($T_{0\text{-}2} \approx 83$ K; Spitzer et al. 1974) of Figure 4. Such distributions do not satisfactorily reproduce our spectrum. We are left with two possibilities: either the observed H_2 is predominantly interstellar with a high b (near 15 km s^{-1} or greater) and corresponding low column density, or it is located near NGC 1535 with a column density of 7.5×10^{17} cm^{-2}–2.5×10^{18} cm^{-2}. For either origin, the characteristic temperature we require is around 300 K.

We cannot discriminate between these possibilities from our data alone. Incorporating *Copernicus* data for a nearby line of sight, however, we conclude it is plausible, and perhaps even likely, that the majority of the detected H_2 is associated with NGC 1535. The line of sight toward the star HD 28497 ($d = 466$ pc) is just 4°.5 away from the direction to NGC 1535. The *Copernicus* H I column density to HD 28497 is $N(H) = 1.6 \times 10^{20}$ cm^{-2} (Bohlin 1975), comparable to that toward NGC 1535 (determined in § 4.2 below). The H_2 toward HD 28497 is distributed in two clouds, with the dominant contribution coming from component A. This component has an uncertain b, 7 km s^{-1} < b < 15 km s^{-1} (York 1976), the upper limit being very close to the b-value determined toward NGC 1535 from atomic species (Luhman & Dinerstein 1990). However, the H_2 column density toward HD 28497 is just 6.6×10^{14} cm^{-2}. We have modeled the H_2 column of component A using the population distribution determined by York (1976) for $J'' = 0$, 1, 3, 4 and an interpolated value of 7.5×10^{13} cm^{-2} for $J'' = 2$. We find that the depth of features in the 980–1020 Å region are practically undetectable at our resolution and signal-to-noise. With such a low column density, the strongest lines are just slightly off the linear portion of the curve of growth so there is little dependence of this result on b value. The H_2 column density toward NGC 1535 is clearly much greater than that toward HD 28497 despite the other similarities. HD 28497 is about 1 kpc nearer than NGC 1535, but there is unlikely to be additional H_2 in the halo beyond HD 28497 since the Galactic H_2 is closely confined to the disk (half thickness scale height of just 70 pc; Scheffler & Elsässer 1988). While changes in line of sight characteristics are known on angular scales smaller than the separation on these two objects (see Meyer & Roth 1991), the halo in this direction appears much less complex than that line of sight. We also note that no high-latitude CO clouds are known anywhere near this line of sight (Magnani, Lada, & Blitz 1986). We conclude that the much greater column of H_2 detected toward the PN is likely associated with it.

In the following sections we consider the implications of our results, assuming the H_2 that we detect is associated with NGC 1535. Even if this is not strictly true, ascribing the observed H_2 to the PN allows us to determine an upper limit to the mass of H_2 that can be present near the PN.

4.1. *Neutral Zone Conditions*

We first estimate the conditions in the neutral (H I + H_2) zone and determine if they are in reasonable agreement with PDR models and with other observations of this PN. In particular we will use relations derived by Jura (1974, 1975b) to make order of magnitude estimates of the density and incident flux in the H_2 zone. The estimate of the incident flux depends on absorption as determined for the square root portion of the curve of growth. This condition is met for nearly all lines in the $J'' = 0$, 1, 2 levels (the levels from which nearly all absorption takes place) at $b = 3$ km s^{-1} and $N(H_2) = 2.5 \times 10^{18}$ cm^{-2}. It is met by many (but not all) similar levels, at $b = 7$ km s^{-1} and $N(H_2) = 7.5 \times 10^{17}$ cm^{-2}. We will estimate conditions for both $b = 3$ km s^{-1} and $b = 7$ km s^{-1}, with the caveat that results at $b = 7$ km s^{-1} are less certain. Throughout, n denotes the usual number density, N refers to column density, and a distance of 1.6 kpc is assumed.

The best fit model at $b = 3$ km s^{-1} has an H_2 column density of 2.5×10^{18} cm^{-2}. The combination of R, the H_2 formation rate on grains, and the hydrogen nuclei density [$n = n(H) + 2n(H_2)$], with a 300 K distribution can be expressed as

$$Rn = 5.5 \times 10^{-9} \frac{N(4)}{N(H)}, \tag{1}$$

where $N(4)$ is the $J'' = 4$ column density (8.2×10^{15} cm^{-2}) and $N(H)$ is the hydrogen column density (1.8×10^{20} cm^{-2}, derived below). Thus, $Rn = 2.5 \times 10^{-13}$ s^{-1} and with a nominal value of $R = 2 \times 10^{-17}$ cm^3 s^{-1} (Jura 1975a), we determine a neutral zone density $n = 1.3 \times 10^4$ cm^{-3}. To estimate the incident flux at the H_2 zone, we recast the expression (equation A8 from Jura 1974) relating I, the average dissociation rate of H_2, and $f = 2n(H_2)/[n(H) + 2n(H_2)]$, the average molecular fraction, as

$$I = \frac{nR}{4.2 \times 10^5} \sqrt{\frac{N}{2f}}. \tag{2}$$

I is directly proportional to the total H_2 absorbed flux rate, β; for a dissociation probability of 0.11 (Jura 1975a), $\beta = 9I$. β in turn is directly proportional to the UV flux, F. The usual parameterization is (Shull & Beckwith 1982) $\beta = \beta_0(F/F_0)$, where $\beta_0 = 5 \times 10^{-10}$ s^{-1} (Jura 1975a) and F_0 is the average interstellar flux near 1000 Å, $F_0 = 3 \times 10^{-8}$ photons cm^{-2} s^{-1} Hz^{-1} (Jura 1974). Using $Rn = 2.5 \times 10^{-13}$ s^{-1}, and $N = 1.85 \times 10^{20}$ cm^{-2} [$= N(H) + 2N(H_2)$], and using $f = 0.03$ determined from our model parameters, we calculate that $I = 3.5 \times 10^{-8}$ s^{-1} and $\beta = 3.1 \times 10^{-7}$ s^{-1}, indicating an incident flux of $627F_0$. We compare this value to our extinction-corrected measurement of 2.5×10^{-11} ergs s^{-1} cm^{-2} Å^{-1} near 1000 Å. The flux near NGC 1535 is

$$\frac{F}{F_0} = \frac{577}{\theta_{30}^2}, \tag{3}$$

where θ_{30} is the angular separation, scaled to 30″, between the central star and the H_2 zone. This separation corresponds to the outer edge of the ionized halo around NGC 1535, a position where H_2 is likely to be located based on IR images of H_2 in other PNs (Beckwith et al. 1978; Zuckerman & Gatley 1988). For the $b = 3$ km s^{-1}, $N(H_2) = 2.5 \times 10^{18}$ cm^{-2} models, the estimate of the incident flux near 1000 Å based on H_2 excitation ($627F_0$) is thus in nominal agreement with the UV flux near the edge of the halo of NGC 1535 ($577F_0$). At $b = 7$ km s^{-1} and with the corresponding lower column density, $N(H_2) = 7.5 \times 10^{17}$ cm^{-2}, we get similar results: $n = 3.7 \times 10^3$ cm^{-3}, about $\frac{1}{3}$ the result for $b = 3$ km s^{-1}, and $F = 331F_0$, again in order-of-magnitude agreement with the available UV flux near NGC 1535. We note that the above

arguments assume a steady state between the formation and destruction of H_2, which almost certainly is not correct; still, we find the order of magnitude agreement to be encouraging.

We also note that our nominal temperature, $T = 300$ K, agrees well with predictions of model PDRs. Sternberg & Dalgarno (1989) present the thermal profile of such a model having $n_T = n(H) + n(H_2) = 1 \times 10^4$ cm^{-3}, practically equal to the 1.3×10^4 cm^{-3} neutral zone density derived above. The model-determined temperature is about 300 K for a range of the incident flux parameter of 10^2–10^5 and for H_2 column depths of 10^{16}–10^{20} cm^{-2}, a range that includes the incident flux and column densities determined above.

These PDR models, as well as those of Burton et al. (1990), make detailed predictions of various IR cooling lines that could be measured toward NGC 1535 to better determine the neutral zone conditions. We mention here only the prediction of IR H_2 emission. Storey (1984) reports an upper limit of less than 1.7×10^{-14} ergs cm^{-2} s^{-1} from the (1–0) $S(1)$ line at 2.12 μm. With a beam size of 14″ × 5″ this equals 1.0×10^{-5} ergs cm^{-2} s^{-1} sr^{-1}. Burton et al. (1990) predict almost exactly this flux for a PDR with density 1×10^4 cm^{-3} for incident UV flux parameters of 10^3–10^5. Based on our data, a more sensitive IR measurement of NGC 1535 may well be able to detect such emission. At a density of 10^3 cm^{-3} (similar to our $b = 7$ km s^{-1} estimate), the predicted flux is reduced by only a factor of 4.

4.2. H_2 *and* H I *Masses*

We can use a simple model to place an upper limit on the H_2 mass associated with NGC 1535. We assume that the molecular gas we see in our spectrum is associated with the PN and lies in a thin, continuous shell at a distance r from the central star. Then

$$M(H_2) = 4\pi r^2 N(H_2) m \, , \tag{4}$$

where m is the mass of an H_2 molecule. We can convert this into a relation between the molecular mass, the distance $d_{1.6}$ (normalized to 1.6 kpc), and θ_{30} as

$$M(H_2) = 1.1 \times 10^{-20} N(H_2) d_{1.6}^2 \theta_{30}^2 \, M_\odot \, . \tag{5}$$

Using our highest value of $N(H_2) = 2.5 \times 10^{18}$ cm^{-2}, and ascribing all of the observed H_2 to the PN, we determine an upper limit to the H_2 mass in NGC 1535 of 0.028 $M_\odot$.

This H_2 mass upper limit is much less than typically estimated from IR measurements of PNs. For instance, Isaacman (1984) derives H_2 masses of six PNs invoking a theory of shock excitation, and finds several tenths of a solar mass to be typical. Using Storey's (1984) IR upper limit and a procedure similar to Isaacman (1984) applied to NGC 1535, we derive an IR upper limit on the H_2 mass of 0.31 $M_\odot$, about 11 times larger than the UV upper limit which we derive for an easily detected H_2 column. Ultraviolet absorption measurements are thus a very sensitive means of detecting the presence of small amounts of H_2.

Another important aspect of the UV/IR comparison, however, is that IR mass estimates are subject to large model-dependent uncertainties that do not affect the UV estimates. IR detection depends on emission from excited states, whether the excitation mechanism is shocks or fluorescence by the UV-bright central star. For shocks, only the possibly small fraction of H_2 behind the shock front will be raised to temperatures of more than 1000 K necessary for excitation. Thus in estimating total H_2 masses, Isaacman (1984) derives preshock (unexcited H_2) to shocked H_2 mass ratios of 100–600. With fluorescence on the other hand, only that H_2 which is exposed to UV flux will fluoresce. Extinction by dust or H_2 self-shielding can limit this process so that most of the H_2 mass still remains unexcited, and so undetected. Whatever the excitation mechanism, one can ask whether there is still a significant, undetected mass of H_2 in NGC 1535 in spite of the upper limit found by Storey (1984). Our UV result establishes that there is very little unexcited H_2 in NGC 1535, the form in which the bulk of the molecular gas must exist.

What is the total amount of neutral gas present in NGC 1535? Direct measurements of nebular H I have been made for only a few PNs (Taylor et al. 1990) and NGC 1535 has not been included so far. However, we may obtain an upper limit to the amount of H I by using the X-ray flux from NGC 1535 detected by the *Exosat* satellite and reported by Apparao & Tarafdar (1989). Assuming a blackbody spectrum, the appropriate instrumental effective area, the measured stellar magnitude, and a neutral hydrogen column toward NGC 1535, Apparao & Tarafdar obtain an X-ray temperature of 79,500 K for NGC 1535. This value is in reasonable agreement with that obtained by Aller (1982) who found that the nebular excitation could be explained by a photoionization source resembling a 70,000 K blackbody to 130 eV. In addition, Patriarchi, Perinotto, & Cerruti-Sola (1989) find a He^+ Zanstra temperatures in the range 73,000–89,000 K, depending on assumptions, and Mendez et al. (1988) find $T_{\rm eff} = 70{,}000$ K from optical line profile fits. Apparao & Tarafdar (1989) derive the H I column from the nebular extinction parameter $c = 0.09$ [$E(B-V) = 0.06$]. This value is an average of extinction measurements derived by different methods (Pottasch 1984). Using the value of 5.8×10^{21} atoms cm^{-2} for each magnitude of $E(B-V)$ (Bohlin, Savage, & Drake 1978; Savage & Mathis 1979) yields a neutral hydrogen column of 3.5×10^{20} cm^{-2} toward NGC 1535. We will assume that of order half of this column is interstellar, a value similar to the *Copernicus* measurement of 1.6×10^{20} cm^{-2} toward HD 28497 (Bohlin 1975). In a manner similar to our estimate of nebular H_2 mass, an upper limit to the H I mass in a shell around NGC 1535 is then given by

$$M(\text{H I}) = 5.4 \times 10^{-21} N(\text{H I}) d_{1.6}^2 \theta_{30}^2 \, M_\odot \, . \tag{6}$$

With $N(\text{H I}) = 1.8 \times 10^{20}$ cm^{-2}, we obtain a somewhat conservative upper limit of 1 $M_\odot$ of neutral H I outside the ionized zone at a radius of 30″. (Note: there is no correlation between H_2 column density and $E(B-V)$ for $E(B-V) \leq 0.1$ [Savage et al. 1977] so no approximate value of H_2 column density can be determined from the extinction to NGC 1535.)

4.3. *Implications*

We now combine our estimates of the neutral mass with those of the ionized nebulosity and the central star mass to determine an upper limit to the progenitor of NGC 1535. The central star mass is 0.65–0.67 $M_\odot$, as determined by atmospheric line analysis (Méndez et al. 1988; Méndez, Kudritzki, & Herrero 1992). The total ionized nebular mass was determined to be 0.13 $M_\odot$ by Sabbadin et al. (1984) and 0.093 $M_\odot$ by Méndez et al. (1992). A small but typical nebular dust mass of 3.2×10^{-4} $M_\odot$ has also been determined from *IRAS* data (Lenzuni, Natta, & Panagia 1989). (The presence of nebular

dust is a likely prerequisite for H_2 formation.) We estimate the remaining neutral mass to be less than 1 $M_\odot$ of H I and $< 0.03 d_{1.6}^2\ M_\odot$ of H_2. The total progenitor mass for NGC 1535 is thus less than 1.8 $M_\odot$.

This upper limit is in general accord with the evolutionary picture that has been developed for NGC 1535. Since NGC 1535 is far off the galactic plane, it's progenitor was probably a Population II object or a member of the extended "thick disk" population (Gilmore & Reid 1983; Reid & Majewski 1993), and thus would be expected to have a relatively low mass. Using the relation between initial and final mass (Iben & Renzini 1983),

$$M_f = 0.53\eta^{-0.082} + 0.15\eta^{-0.35}(M_i - 1) \quad (7)$$

and a value for the mass-loss parameter, $\eta = \frac{1}{3}$ (Heap & Augensen 1987), we expect the progenitor of NGC 1535 to have a mass of 1.2–1.4 $M_\odot$, corresponding to a current central star mass of 0.63 $M_\odot$ (Heap & Augensen 1987) or 0.67 $M_\odot$ (Méndez et al. 1988). The models of Schönberner (1987) are consistent with this picture, showing a 1.4 $M_\odot$ progenitor leaving a PN central star of 0.64 $M_\odot$. These values are certainly consistent with our upper limit of 1.8 $M_\odot$.

The evolutionary models do not address the form of the neutral mass, but only indicate the likely total amount. Using our nominal range of H_2 column density (7.5×10^{17}–2.5×10^{18} cm^{-2}) and our estimated H I column density, the N(H I)/N(H_2) ratio is 72–240. This ratio is in marked contrast to the originally expelled stellar wind from NGC 1535 which should have been largely H_2 (Howe et al. 1992). It is also considerably larger than the canonical ISM ratio of 10 (Savage & Mathis 1979); the neutral zone around NGC 1535 thus may be relatively depleted in H_2 compared with the original stellar wind or the current ISM [depending on the actual value of N(H I)]. Such a condition would be expected due to progressive photodissociation of the original H_2 and conversion to H I. Greenhouse, Hayward, & Thronson (1988) find a similar result for NGC 6720, a PN with a central star mass close to that of NGC 1535 but which is more evolved.

Hippelein, Baessgen, & Grewing (1985) hypothesize that a massive neutral shell must surround the ionized halo in order to account for the lack of detected mass in such PNs. Halo measurements have shown typical ionized H densities of 100 cm^{-3} (Jewitt, Danielson, & Kupferman 1986). At typical nebular temperatures of 10,000 K, gas at this density would be in thermal equilibrium with a neutral shell at 300 K with a density of 3×10^3 cm^{-3}, comparable to our $b = 7$ km s^{-1} result. Hence, such a neutral cocoon in thermal pressure equilibrium with the observed halo might plausibly define the sharp halo edge, as described by Hippelein, Baessgen, & Grewing (1985).

However, the absence of any optical halo outside that shown in Figure 1, as recently reported by Balick et al. (1992), would seem to indicate that any such neutral cocoon is thoroughly shielded from ionizing photons. This conclusion is at odds with the findings of Méndez et al. (1992), who show (among other things) that only 7% of the ionizing flux from the central star in NGC 1535 is intercepted by the nebula (see their Table 4). This "density-bounded" picture would preclude the presence of a substantial neutral halo in NGC 1535. The HUT observation reported above places hard limits on the amount of molecular gas that can be present. Future work may restrict the upper limit on neutral atomic material as well, and help resolve the above discrepancy.

If future measurements restrict the neutral mass well below 1 $M_\odot$, this may cause a discrepancy with a progenitor as massive as 1.2–1.4 $M_\odot$. We note that Jura & Kleinmann (1992) identify a population of short period Mira variables with a scale height of 500–600 pc and main-sequence progenitors of $\leq 1.1\ M_\odot$, which may prove to be of interest in future discussions of the NGC 1535 progenitor.

5. SUMMARY

We have detected H_2 Lyman and Werner band absorption toward the galactic halo planetary nebula NGC 1535 and modeled its characteristics. This detection is the first such measurement for any PN central star, and demonstrates the expanded range of objects which can be used as UV probes of the ISM with current instrumentation.

We find that an H_2 population distribution over rotational levels characterized by a single temperature near 300 K reproduces our data over a range of Doppler parameter b, from 3–15.8 km s^{-1}. Two-temperature distributions that approximate such a 300 K distribution can also reproduce our observation. An upper limit to the H_2 column density of 2.5×10^{18} cm^{-2} is determined. An interstellar origin for the H_2 is possible but only if the b-value is ≥ 15 km s^{-1}. However, comparison to the nearby line of sight to HD 28497 observed with *Copernicus* suggests that the observed H_2 is more likely associated with NGC 1535.

The particle density and illuminating flux we infer are in reasonable agreement with conditions expected near NGC 1535. This conclusion is consistent with previous upper limits on the IR emission from NGC 1535 but is not consistent with shock-excited nebular H_2 at temperatures of 1000–2000 K. Since the UV transitions we sample are ground-state-connected, we can place a more stringent, less model dependent upper limit on the H_2 mass in NGC 1535 of less than $0.03 d_{1.6}^2$ $M_\odot$. We also estimate an upper limit of 1 $M_\odot$ to the mass of H I in NGC 1535. The neutral shell around NGC 1535 thus may be greatly depleted in H_2, indicating substantial dissociation from any original H_2-rich superwind, as proposed by Howe et al. (1992). Combined with determinations of the central star mass and ionized nebular mass, we determine an upper limit to the progenitor star mass less than 1.8 $M_\odot$, a value which is consistent with the general picture of the evolutionary status of NGC 1535.

A 21 cm H I measurement would be of considerable value in clarifying the amount of H I mass present, which appears to form the bulk of the neutral material in NGC 1535. Additional IR emission measurements of H_2 using the more sensitive detectors now available would also be of great value, as they could provide a combined IR/UV picture of H_2 in a PN and determine the spatial distribution of the excited neutral component. Such measurements could also verify the fluorescent nature of H_2 excitation.

We thank the Mission Operations Support group at the Marshall Space Flight Center for their support during the Astro-1 mission. We also thank the crew of the Astro-1 mission for their efforts to overcome problems encountered during the flight in order to obtain these data. We thank Harriet Dinerstein, Patrick Huggins, and Sara Heap for useful conversations. Bruce Balick provided access to optical CCD images of NGC 1535, for which we are grateful. The Hopkins Ultraviolet Telescope project is supported by NASA contract NAS 5-27000 to The Johns Hopkins University.

REFERENCES

Adam, J., & Köppen, J. 1985, A&A, 142, 461
Aller, L. H. 1982, Ap&SS, 83, 225
Apparao, K. M. V., & Tarafdar, S. P. 1989, ApJ, 344, 826
Balick, B. 1987, AJ, 94, 671
Balick, B., Gonzalez, G., Frank, A., & Jacoby, G. 1992, ApJ, 392, 582
Beckwith, S., Neugebauer, G., Becklin, E., & Matthews, K. 1980, ApJ, 85, 886
Beckwith, S., Persson, S. E., & Gatley, I. 1978, ApJ, 219, L33
Bohlin, R. C. 1975, ApJ, 200, 402
Bohlin, R. C., Savage, B. D., & Drake, J. F. 1978, ApJ, 224, 132
Burton, M. G., Hollenbach, D. J., & Tielens, A. G. G. M. 1990, ApJ, 365, 620
Cartwright, D. C., & Drapatz, S. 1970, A&A, 4, 443
Clegg, R. E. S., & Middlemass, D. 1987, MNRAS, 228, 759
Davidsen, A. F., et al. 1992, ApJ, 392, 264
Dinerstein, H. L., Lester, D. F., Carr, J. S., & Harvey, P. M. 1988, ApJ, 327, L27
Gilmore, G., & Reid, N. 1983, MNRAS, 202, 1025
Greenhouse, M. A., Hayward, T. L., & Thronson, Jr., H. A. 1988, ApJ, 325, 604
Harris, A. W., & Bromage, G. E. 1984, MNRAS, 208, 941
Heap, S. R., & Augensen, H. J. 1987, ApJ, 313, 268
Hippelein, H. H., Baessgen, M., & Grewing, M. 1985, A&A, 152, 213
Howe, D. A., Millar, T. J., & Williams, D. A. 1992, MNRAS, 255, 217
Huggins, P. J., & Healy, A. P. 1989, ApJ, 346, 201
Iben, I., & Renzini, A. 1983, ARA&A, 21, 271
Isaacman, R. 1984, A&A, 130, 151
Jewitt, D. C., Danielson, G. E., & Kupferman, P. N. 1986, ApJ, 302, 727
Jura, M. 1974, ApJ, 191, 375
———. 1975a, ApJ, 197, 575
———. 1975b, ApJ, 197, 581
Jura, M., & Kleinmann, S. G. 1992, ApJS, 79, 105
Kimble, R. A., et al. 1993, ApJ, 404, 663
Kriss, G. A. 1995, in ASP Conf. Ser., Proceedings of The Third Conference on Astrophysics Data Analysis and Software Systems, ed. D. Crabtree (San Francisco: ASP), in press
Lenzuni, P., Natta, A., & Panagia, N. 1989, ApJ, 345, 306
Luhman, M., & Dinerstein, H. L. 1990, BAAS, 22, 813
Longo, R., Stalio, R., Polidan, R., & Rossi, L. 1989, ApJ, 339, 474
Magnani, L., Lada, E. A., & Blitz, L. 1986, ApJ, 301, 395
Méndez, R. H., Kudritzki, R. P., & Herrero, A. 1992, A&A, 260, 329
Méndez, R. H., Kudritzki, R. P., Herrero, A., Husfeld, D., & Groth, H. G. 1988, A&A, 190, 113
Meyer, D. M., & Roth, K. C. 1991, ApJ, 383, L41
Morton, D. C. 1991, ApJS, 77, 119
Morton, D. C., & Dinerstein, H. L. 1976, ApJ, 204, 1
Patriarchi, P., Perinotto, M., & Cerruti-Sola, M. 1989, ApJ, 345, 327
Polidan, R. S., & Holberg, J. B. 1985, in IAU Symp. 111, Calibration of Fundamental Stellar Quantities, ed. D. S. Hayes, L. E. Pasinetti, & A. G. Davis Philip (Dordrecht: Reidel), 479
Pottasch, S. R. 1984, Planetary Nebulae (Dordrecht: Reidel)
Reid, N., & Majewski, S. R. 1993, ApJ, 409, 635
Sabbadin, F., Bianchini, A., & Hamzaoglu, E. 1984, A&A, 136, 193
Sahai, R., Wootten, A., Schwarz, H. E., & Clegg, R. E. S. 1991, A&A, 251, 560
Savage, B. D., Bohlin, R. C., Drake, J. F., & Budich, W. 1977, ApJ, 216, 291
Savage, B. D., & Mathis, J. S. 1979, ARA&A, 17, 73
Scheffler, H., & Elsässer, H. 1988, Physics of the Galaxy and Interstellar Matter (Berlin: Springer)
Schönberner, D. 1981, A&A, 103, 119
———. 1983, ApJ, 272, 708
———. 1987, in Late Stages of Stellar Evolution, ed. S. Kwok & S. R. Pottasch (Dordrecht: Reidel), 337
Seaton, M. J. 1979, MNRAS, 187, 73P
Shull, J. M., & Beckwith, S. 1982, ARA&A, 20, 163
Spitzer, Jr., L., & Cochran, W. D. 1973, ApJ, L23
Spitzer, Jr., L., Cochran, W. D., & Hirshfeld, A. 1974, ApJS, 28, 373
Sternberg, A., & Dalgarno, A. 1989, ApJ, 338, 197
Storey, J. W. V. 1984, MNRAS, 206, 521
Taylor, A. R., Gussie, G. T., & Pottasch, S. R. 1990, ApJ, 351, 515
Treffers, R. R., Fink, U., Larson, H. P., & Gautier, T. N., III. 1976, ApJ, 209, 793
York, D. G. 1976, ApJ, 204, 750
Zuckerman, B., & Gatley, I. 1988, ApJ, 324, 501